Supporting Information

How plasma reaction conditions affect the optimal catalyst: A microkinetic study of plasma-catalytic CO_2 splitting

Björn Loenders [1,2,*], Roel Michiels[1,2] and Annemie Bogaerts[1,2]

1) Research group PLASMANT, Department of Chemistry, University of Antwerp, Universiteitsplein 1, B-2610 Wilrijk-Antwerp, Belgium
2) Electrification Institute, University of Antwerp, Olieweg 97, 2020 Antwerp, Belgium.

* Corresponding author, E-mail address: bjorn.loenders@uantwerpen.be

S1. Rate coefficients used in the model

With p_{ref} = 10^5 Pa (1 bar) and c^R and c^L are the stoichiometry coefficients of the products and the reactants, respectively. The second factor in Eq. S1 is required to keep the units of K_{eq} consistent with those of the rate coefficients. The Gibbs free energy ΔG is calculated using the NASA Polynomials.[1,2]

Table S1 lists the gas phase reactions included in the model, along with their rate coefficients. Some of these rate coefficients are calculated from the rate coefficients of the corresponding reverse reaction and the equilibrium constant via detailed balancing. The equilibrium constant used for detailed balancing is calculated according to:

$$K_{eq} = \exp\left(-\frac{\Delta G}{R_{gas}T_{gas}}\right) \cdot \left(\frac{p_{ref}}{R_{gas}T_{gas}}\right)^{\Sigma c^R - \Sigma c^L} \quad \text{(S1)}$$

With p_{ref} = 10^5 Pa (1 bar) and c^R and c^L are the stoichiometry coefficients of the products and the reactants, respectively. The second factor in Eq. S1 is required to keep the units of K_{eq} consistent with those of the rate coefficients. The Gibbs free energy ΔG is calculated using the NASA Polynomials.[1,2]

Table S1. List of gas phase reactions included in the model, with their corresponding rate coefficients.

Reaction	Rate coefficient[a]	Ref.
$e^- + O \rightarrow e^- + e^- + O^+$	$f(\sigma)$	3
$e^- + O^- \rightarrow e^- + e^- + O$	$f(\sigma)$	4
$e^- + O_2 \rightarrow e^- + e^- + O_2^+$	$f(\sigma)$	3
$e^- + O_2 \rightarrow e^- + e^- + O + O^+$	$f(\sigma)$	5

$e^- + O_2 \rightarrow e^- + O + O$	$f(\sigma)$	3
$e^- + O_2 \rightarrow e^- + O + O(1D)$	$f(\sigma)$	3
$e^- + O \rightarrow e^- + O(1D)$	$f(\sigma)$	3
$e^- + O_2 \rightarrow O + O^-$	$f(\sigma)$	3
$e^- + O_3 \rightarrow O + O_2^-$	$f(\sigma)$	4
$e^- + O_3 \rightarrow O_2 + O^-$	$f(\sigma)$	4
$CO_2 + e^- \rightarrow CO_2^+ + e^- + e^-$	$f(\sigma)$	3
$CO_2 + e^- \rightarrow CO(a3P) + O + e^-$	$f(\sigma)$	6
$CO_2 + e^- \rightarrow CO + O(1D) + e^-$	$f(\sigma)$	6
$CO_2 + e^- \rightarrow CO + O^-$	$f(\sigma)$	7
$CO + e^- \rightarrow CO^+ + e^- + e^-$	$f(\sigma)$	3
$CO + e^- \rightarrow CO(a3P) + e^-$	$f(\sigma)$	3
$CO + e^- \rightarrow C + O^-$	$f(\sigma)$	3
$CO + e^- \rightarrow C + O + e^-$	$f(\sigma)$	3
$C + e^- \rightarrow C^+ + e^- + e^-$	$f(\sigma)$	4
$M + e^- + O \rightarrow M + O^-$	1×10^{-31}	8,9
$M + e^- + O_2 \rightarrow M + O_2^-$	1×10^{-31}	8,9
$e^- + e^- + O^+ \rightarrow e^- + O$	$7 \times 10^{-20} \cdot \left(\frac{3.0 \times 10^2}{T_e}\right)^{4.5}$	8
$M + e^- + O^+ \rightarrow M + O$	$6 \times 10^{-27} \cdot \left(\frac{3.0 \times 10^2}{T_e}\right)^{1.5}$	8,9
$e^- + e^- + O_2^+ \rightarrow e^- + O_2$	$1 \times 10^{-19} \cdot \left(\frac{3.0 \times 10^2}{T_e}\right)^{4.5}$	9
$M + e^- + O_2^+ \rightarrow M + O_2$	$6 \times 10^{-27} \cdot \left(\frac{3.0 \times 10^2}{T_e}\right)^{1.5}$	8,9
$e^- + O_2^+ \rightarrow O + O$	$2.7 \times 10^{-7} \cdot \left(\frac{3.0 \times 10^2}{T_e}\right)^{0.7}$	8
$M + O + O \rightarrow M + O_2$	$5.2 \times 10^{-35} \cdot \exp\left(\frac{9 \times 10^2}{T_{gas}}\right)$	10
$O + O \rightarrow e^- + O_2^+$	$\frac{1.12 \times 10^{13}}{N_A} \cdot \exp\left(\frac{-8.06 \times 10^4}{T_{gas}}\right)$	11
$O + O^- \rightarrow e^- + O_2$	2.3×10^{-10}	12
$M + O + O^+ \rightarrow M + O_2^+$	1×10^{-29}	8,9
$O + O_2^- \rightarrow O_2 + O^-$	3.3×10^{-10}	8,9
$O + O_2^- \rightarrow e^- + O_3$	1.5×10^{-10}	8,9

$O + O_3 \rightarrow O_2 + O_2$	$8 \times 10^{-12} \cdot \exp\left(\frac{-2.060 \times 10^3}{T_{gas}}\right)$	13
$M + O + O_2 \rightarrow M + O_3$	$5.4 \times 10^{-34} \cdot \left(\frac{3.0 \times 10^2}{T_{gas}}\right)^{1.9}$	8
$O_2 + O^+ \rightarrow O + O_2^+$	$2 \times 10^{-11} \cdot \left(\frac{3.0 \times 10^2}{T_{gas}}\right)^{0.5}$	8
$O_3 + O^+ \rightarrow O_2 + O_2^+$	1×10^{-10}	8,9
$O^- + O^+ \rightarrow O + O$	$2 \times 10^{-7} \cdot \left(\frac{3.0 \times 10^2}{T_{gas}}\right)^{0.5}$	9
$O_2^- + O^+ \rightarrow O + O_2$	$2 \times 10^{-7} \cdot \left(\frac{3.0 \times 10^2}{T_{gas}}\right)^{0.5}$	9
$M + O_2^- + O^+ \rightarrow M + O + O_2$	$2 \times 10^{-25} \cdot \left(\frac{3.0 \times 10^2}{T_{gas}}\right)^{2.5}$	9
$M + O^- + O^+ \rightarrow M + O + O$	$2 \times 10^{-25} \cdot \left(\frac{3.0 \times 10^2}{T_{gas}}\right)^{2.5}$	9
$M + O_2^- + O^+ \rightarrow M + O_3$	$2 \times 10^{-25} \cdot \left(\frac{3.0 \times 10^2}{T_{gas}}\right)^{2.5}$	9
$M + O^- + O^+ \rightarrow M + O_2$	$2 \times 10^{-25} \cdot \left(\frac{3.0 \times 10^2}{T_{gas}}\right)^{2.5}$	9
$O_2^+ + O^- \rightarrow O + O + O$	1×10^{-7}	9
$O_2^+ + O^- \rightarrow O + O_2$	$2 \times 10^{-7} \cdot \left(\frac{3.0 \times 10^2}{T_{gas}}\right)^{0.5}$	9
$O_2 + O^- \rightarrow e^- + O_3$	5×10^{-15}	8,9
$O_3 + O^- \rightarrow e^- + O_2 + O_2$	3×10^{-10}	8,14
$M + O^- \rightarrow M + e^- + O$	$6.9 \times 10^{-10} \cdot \left(\frac{3.0 \times 10^2}{T_{gas}}\right)^{-0.5}$	15
$M + O_2^+ + O^- \rightarrow M + O + O_2$	$2 \times 10^{-25} \cdot \left(\frac{3.0 \times 10^2}{T_{gas}}\right)^{2.5}$	9
$M + O_2^+ + O^- \rightarrow M + O_3$	$2 \times 10^{-25} \cdot \left(\frac{3.0 \times 10^2}{T_{gas}}\right)^{2.5}$	9
$O_2 + O_2 \rightarrow O + O_3$	$2 \times 10^{-11} \cdot \exp\left(\frac{-4.980 \times 10^4}{T_{gas}}\right)$	8
$M + O_2 \rightarrow M + O + O$	$3 \times 10^{-6} \cdot T_{gas}^{-1} \cdot \exp\left(\frac{-5.938 \times 10^4}{T_{gas}}\right)$	10

$M + O_2^- + O_2^+ \rightarrow M + O_2 + O_2$	$2 \times 10^{-25} \cdot \left(\frac{3.0 \times 10^2}{T_{gas}}\right)^{2.5}$	9
$O_2^- + O_2^+ \rightarrow O + O + O_2$	1×10^{-7}	9
$O_2^- + O_2^+ \rightarrow O_2 + O_2$	$2 \times 10^{-7} \cdot \left(\frac{3.0 \times 10^2}{T_{gas}}\right)^{0.5}$	9,16
$M + O_2^- \rightarrow M + e^- + O_2$	$2 \times 10^{-10} \cdot \left(\frac{3.0 \times 10^2}{T_{gas}}\right)^{-0.5}$	15
$M + O_3 \rightarrow M + O + O_2$	$6.6 \times 10^{-10} \cdot \exp\left(\frac{-1.160 \times 10^4}{T_{gas}}\right)$	8
$CO^+ + e^- \rightarrow C + O$	$6.8 \times 10^{-7} \cdot \left(\frac{T_e}{3.0 \times 10^2}\right)^{-0.4}$	17
$CO_2^+ + e^- \rightarrow CO + O$	$0.5 \cdot 3.4 \times 10^{-6} \cdot \left(\frac{T_e}{3.0 \times 10^2}\right)^{-0.4}$	17
$CO_2^+ + e^- \rightarrow C + O_2$	$0.5 \cdot 3.4 \times 10^{-6} \cdot \left(\frac{T_e}{3.0 \times 10^2}\right)^{-0.4}$	17
$CO + O \rightarrow CO_2^+ + e^-$	$\frac{1.12 \times 10^{13}}{N_A} \cdot \exp\left(\frac{-8.06 \times 10^4}{T_{gas}}\right)$	18 [b]
$C + O_2 \rightarrow CO_2^+ + e^-$	$\frac{1.12 \times 10^{13}}{N_A} \cdot \exp\left(\frac{-8.06 \times 10^4}{T_{gas}}\right)$	18 [b]
$C + O \rightarrow CO^+ + e^-$	$\frac{5.28 \times 10^{12}}{N_A} \cdot \exp\left(\frac{-3.2 \times 10^4}{T_{gas}}\right)$	11,18
$CO^+ + e^- + e^- \rightarrow CO + e^-$	$1 \times 10^{-19} \cdot \left(\frac{3.0 \times 10^2}{T_e}\right)^{4.5}$	9 [c]
$M + CO^+ + e^- \rightarrow M + CO$	$6 \times 10^{-27} \cdot \left(\frac{3.0 \times 10^2}{T_e}\right)^{1.5}$	9 [d]
$CO_2^+ + e^- + e^- \rightarrow CO_2 + e^-$	$1 \times 10^{-19} \cdot \left(\frac{3.0 \times 10^2}{T_e}\right)^{4.5}$	9 [c]
$M + CO_2^+ + e^- \rightarrow M + CO_2$	$6 \times 10^{-27} \cdot \left(\frac{3.0 \times 10^2}{T_e}\right)^{1.5}$	9 [d]
$M + C + O \rightarrow M + CO$	$9.1 \times 10^{-22} \cdot T_{gas}^{-3.08} \cdot \exp\left(\frac{-2.114 \times 10^3}{T_{gas}}\right)$	17
$C + O_2 \rightarrow CO + O$	$\frac{1.2 \times 10^{14}}{N_A} \cdot \exp\left(\frac{-2.01 \times 10^3}{T_{gas}}\right)$	19
$M + C + O^+ \rightarrow M + CO^+$	$1 \times 10^{-19} \cdot T_{gas}^{-3.08} \cdot \exp\left(\frac{-2.114 \times 10^3}{T_{gas}}\right)$	20
$C + O_2^+ \rightarrow CO^+ + O$	5.2×10^{-11}	21

$C + O_2^+ \rightarrow C^+ + O_2$	5.2×10^{-11}	21
$C + O^- \rightarrow CO + e^-$	5×10^{-10}	21
$M + C^+ + O \rightarrow M + CO^+$	$1 \times 10^{-19} \cdot T_{gas}^{-3.08} \cdot \exp\left(\frac{-2.114 \times 10^3}{T_{gas}}\right)$	20
$C^+ + O_2 \rightarrow CO + O^+$	$6.2 \times 10^{-1} \cdot 9.9 \times 10^{-10}$	22
$C^+ + O_2 \rightarrow CO^+ + O$	$3.8 \times 10^{-1} \cdot 9.9 \times 10^{-10}$	22
$CO_2 + O \rightarrow CO + O_2$	$\frac{1.7 \times 10^{13}}{N_A} \cdot \exp\left(\frac{-2.65 \times 10^4}{T_{gas}}\right)$	17
$CO_2 + O^+ \rightarrow CO_2^+ + O$	$0.5 \cdot 9 \times 10^{-10}$	22
$CO_2 + O^+ \rightarrow CO + O_2^+$	$0.5 \cdot 9 \times 10^{-10}$	22
$M + CO + O \rightarrow M + CO_2$	$8.3 \times 10^{-34} \cdot \exp\left(\frac{-1.51 \times 10^3}{T_{gas}}\right)$	10
$CO + O_2 \rightarrow CO_2 + O$	$4.2 \times 10^{-12} \cdot \exp\left(\frac{-2.4 \times 10^4}{T_{gas}}\right)$	10
$CO + O_3 \rightarrow CO_2 + O_2$	4×10^{-25}	23
$CO + O^+ \rightarrow CO^+ + O$	$2 \times 10^{-11} \cdot \left(\frac{T_{gas}}{5 \times 10^3}\right)^{0.5} \cdot \exp\left(\frac{-4.58 \times 10^3}{T_{gas}}\right)$	20
$CO + O^- \rightarrow CO_2 + e^-$	$6 \times 10^{-10} \cdot \left(\frac{T_{gas}}{3 \times 10^2}\right)^{-0.39}$	24
$CO_2^+ + O \rightarrow CO_2 + O^+$	$0.37 \cdot 2.6 \times 10^{-10}$	22
$CO_2^+ + O \rightarrow CO + O_2^+$	$0.63 \cdot 2.6 \times 10^{-10}$	22
$CO_2^+ + O_2 \rightarrow CO_2 + O_2^+$	5.3×10^{-11}	24
$CO^+ + O \rightarrow CO + O+$	1.4×10^{-10}	25
$CO^+ + O_2 \rightarrow CO + O_2^+$	1.2×10^{-10}	26
$C + CO_2 \rightarrow CO + CO$	1×10^{-15}	27
$CO_2 + C^+ \rightarrow CO + CO^+$	1.1×10^{-9}	28
$C + CO^+ \rightarrow CO + C^+$	1.1×10^{-10}	21
$M + CO_2 \rightarrow M + CO + O$	$\frac{3.65 \times 10^{14}}{N_A} \cdot \exp\left(\frac{-5.2525 \times 10^4}{T_{gas}}\right)$	29
$CO_2 + CO^+ \rightarrow CO + CO_2^+$	1×10^{-9}	26
$M + CO \rightarrow M + C + O$	$1.46 \times 10^6 \cdot T_{gas}^{-3.52} \cdot \exp\left(\frac{-1.287 \times 10^5}{T_{gas}}\right)$	17
$CO(a3P) + O_2 \rightarrow CO + O_2$	5.0×10^{-11}	30
$CO(a3P) + O_2 \rightarrow CO + O + O$	5.0×10^{-11}	30
$CO(a3P) + O_2 \rightarrow CO_2 + O$	3.0×10^{-11}	30
$CO(a3P) + CO \rightarrow CO + CO$	1.4×10^{-10}	30

$CO(a3P) + CO \rightarrow CO_2 + C$	1.4×10^{-12}	30
$CO(a3P) + CO_2 \rightarrow CO + CO_2$	1.5×10^{-11}	30
$CO(a3P) + CO_2 \rightarrow CO + CO + O$	1.5×10^{-11}	30
$O + O(1D) \rightarrow O + O$	8.0×10^{-12}	31
$CO + O(1D) \rightarrow CO + O$	8.0×10^{-11}	32
$O_2 + O(1D) \rightarrow O_2 + O$	$0.312 \times 10^{-10} \cdot \exp\left(\frac{7.00 \times 10^{1}}{T_{gas}}\right)$	33
$CO_2 + O(1D) \rightarrow CO_2 + O$	$0.74 \times 10^{-10} \cdot \exp\left(\frac{1.33 \times 10^{2}}{T_{gas}}\right)$	33
$CO_2^+ + CO_3^- \rightarrow CO_2 + CO_2 + O$	5.0×10^{-7}	34
$CO + CO_3^- \rightarrow CO_2 + CO_2 + e^-$	5.0×10^{-13}	35
$CO_4^- + O \rightarrow CO_3^- + O_2$	$0.333 \cdot 1.4 \times 10^{-10}$	22
$CO_3^- + O_2^+ \rightarrow CO_2 + O + O_2$	3.0×10^{-7}	34
$CO_3^- + O \rightarrow CO_2 + O_2^-$	8.0×10^{-11}	35
$M + CO_2 + O^- \rightarrow M + CO_3^-$	9.0×10^{-29}	35
$M + CO_2 + O_2^- \rightarrow M + CO_4^-$	4.7×10^{-29}	22
$CO_4^- + O \rightarrow CO_2 + O_2 + O^-$	$0.333 \cdot 1.4 \times 10^{-10}$	22
$CO_4^- + O_2^+ \rightarrow CO_2 + O_2 + O_2$	3.0×10^{-7}	34
$CO_2^+ + CO_4^- \rightarrow CO_2 + CO_2 + O_2$	5.0×10^{-7}	34
$CO + O \rightarrow C + O_2$	$k_{rev} \cdot K_{eq}$	e
$CO_2 + O_2 \rightarrow CO + O_3$	$k_{rev} \cdot K_{eq}$	e
$CO + CO \rightarrow C + CO_2$	$k_{rev} \cdot K_{eq}$	e
$CO_2 + O + O_2 \rightarrow CO_3^- + O_2^+$	$k_{rev} \cdot K_{eq}$	e
$CO_2 + O_2^- \rightarrow CO_3^- + O$	$k_{rev} \cdot K_{eq}$	e
$M + CO_3^- \rightarrow M + CO_2 + O^-$	$k_{rev} \cdot K_{eq}$	e

a) Units are s^{-1}, $cm^3\ s^{-1}$ or $cm^6\ s^{-1}$ for unimolecular, bimolecular or trimolecular gas phase reactions, respectively.

b) Estimated: equal to $O + O \rightarrow O_2^+ + e^-$

c) Estimated: equal to $A^+ + e^- + e^- \rightarrow A + e^-$

d) Estimated: equal to $A^+ + e^- + M \rightarrow A + M$

e) Calculated via detailed balancing.

S2. Electron impact reactions included in the model

Table S2. List of the electron impact reactions included in the calculation of the electron energy distribution function.

Electron impact reaction	Ref.
$C + e^- \rightarrow C^+ + e^- + e^-$	4
$C + e^- \rightarrow C + e^-$ (effective)	4
$C + e^- \rightarrow C(1D) + e^-$	4
$C + e^- \rightarrow C(1S) + e^-$	4
$CO + e^- \rightarrow CO + e^-$ (elastic)	3
$CO + e^- \rightarrow CO(v_n) + e^-$ (with n = 1-10)	3
$CO + e^- \rightarrow CO(a3P) + e^-$	3
$CO + e^- \rightarrow CO(a'3Su+) + e^-$	3
$CO + e^- \rightarrow CO(A1P) + e^-$	3
$CO + e^- \rightarrow CO(b3Su+) + e^-$	3
$CO + e^- \rightarrow CO(B1Su+) + e^-$	3
$CO + e^- \rightarrow CO(C1Su+) + e^-$	3
$CO + e^- \rightarrow CO(E1P) + e^-$	3
$CO + e^- \rightarrow C + O + e^-$	3
$CO + e^- \rightarrow C + O^-$	3
$CO + e^- \rightarrow CO^+ + e^- + e^-$	3
$CO_2 + e^- \rightarrow CO_2(v_{010}) + e^-$	3
$CO_2 + e^- \rightarrow CO_2(v_{020}) + e^-$	3
$CO_2 + e^- \rightarrow CO_2(v_{100}) + e^-$	3
$CO_2 + e^- \rightarrow CO_2(v_{030+110}) + e^-$	3
$CO_2 + e^- \rightarrow CO_2(v_{001}) + e^-$	3
$CO_2 + e^- \rightarrow CO_2(v_{040+120+011}) + e^-$	3
$CO_2 + e^- \rightarrow CO_2(X,v_{200}) + e^-$	3
$CO_2 + e^- \rightarrow CO_2(X,v_{050+210+130+021+101}) + e^-$	3
$CO_2 + e^- \rightarrow CO_2(X,v_{300}) + e^-$	3
$CO_2 + e^- \rightarrow CO_2(X,v_{060+220+140}) + e^-$	3
$CO_2 + e^- \rightarrow CO_2(X,v_{0n0+n00}) + e^-$	3
$CO_2 + e^- \rightarrow CO_2(E1) + e^-$	3
$CO_2 + e^- \rightarrow CO_2(E2) + e^-$	3
$CO_2 + e^- \rightarrow CO_2 + e^-$ (effective)	3

$CO_2 + e^- \rightarrow CO + O(1D) + e^-$	6
$CO_2 + e^- \rightarrow CO(a3P) + O + e^-$	6
$CO_2 + e^- \rightarrow CO_2^+ + e^- + e^-$	3
$CO_2 + e^- \rightarrow CO + O^-$	7
$O + e^- \rightarrow O + e^-$ (elastic)	3
$O + e^- \rightarrow O(1D) + e^-$	3
$O + e^- \rightarrow O(1S) + e^-$	3
$O + e^- \rightarrow O(4S0) + e^-$	3
$O + e^- \rightarrow O(2D0) + e^-$	3
$O + e^- \rightarrow O(2P0) + e^-$	3
$O + e^- \rightarrow O(3P0) + e^-$	3
$O + e^- \rightarrow O^+ + e^- + e^-$	3
$O_2 + e^- \rightarrow O_2(v_n) + e^-$ (n = 1-4)	3
$O_2 + e^- \rightarrow O_2(a1Dg) + e^-$	3
$O_2 + e^- \rightarrow O_2(b1Sg+) + e^-$	3
$O_2 + e^- \rightarrow O_2(A3Su+, C3Du, c1Su-) + e^-$	3
$O_2 + e^- \rightarrow O_2(9.97eV) + e^-$	3
$O_2 + e^- \rightarrow O_2(14.7eV) + e^-$	3
$O_2 + e^- \rightarrow O_2 + e^-$ (effective)	3
$O_2 + e^- \rightarrow O_2^+ + e^- + e^-$	3
$O_2 + e^- \rightarrow O + O^+ + e^- + e^-$	5
$O_2 + e^- \rightarrow O + O^-$	3
$O_2 + e^- \rightarrow O + O + e^-$	3
$O_2 + e^- \rightarrow O + O(1D) + e^-$	3
$O_3 + e^- \rightarrow O_3 + e^-$ (effective)	4
$O_3 + e^- \rightarrow O + O_2^-$	4
$O_3 + e^- \rightarrow O_2 + O^-$	4
$O^- + e^- \rightarrow O + e^- + e^-$	4

S3. Surface reactions on glass

Table S3. List of the surface reactions included in the model for glass.

Reaction[a,b]
$O + *^{p} \rightarrow O*^{p}$
$O + *^{c} \rightarrow O*^{c}$
$O*^{p} + *^{c} \rightarrow *^{p} + O*^{c}$
$O*^{p} \rightarrow O + *^{p}$
$O*^{c} \rightarrow O + *^{c}$
$O*^{p} + O*^{c} \rightarrow O_2 + *^{p} + *^{c}$
$O + O*^{p} \rightarrow O_2 + *^{p}$
$O + O*^{c} \rightarrow O_2 + *^{c}$
$CO + O*^{p} \rightarrow CO_2 + *^{p}$
$CO + O*^{c} \rightarrow CO_2 + *^{c}$

a) Superscripts p and c refer to physisorption and chemisorption sites, respectively.

b) For the corresponding rate coefficients, see sections 2.2.4 and 2.2.6 in the main paper.

S4. Effect of varying the parameters governing the glass surface kinetics

In this section we illustrate the possible impact of uncertainties regarding the main parameters that govern the glass surface kinetics. We therefore vary the values of these parameters and observe how the CO and O_2 mole fractions are affected for a CO_2 plasma afterglow at 500 K, 5 mbar and a flow rate of 100 sccm. We study the following parameters: the fraction of chemisorption sites f_c, the pre-exponential factor for desorption ν_d, and the activation barriers for recombination to O_2 and CO_2 ($E_{r,\,O+O}$ and $E_{r,\,CO+O}$, respectively).

Figure S1 shows the effect of varying the fraction of chemisorption sites f_c. The default value used in the main paper is $f_c = 0.002$, so we study here the effect of both increasing and reducing f_c by a factor 10. As can be seen, this causes a strong change in the time required for the O_2 and CO mole fractions to stabilize (which happens when the O atoms in the gas phase are depleted). Indeed, the recombination of O atoms on the glass surface occurs predominantly via an L-R reaction between a chemisorbed O* atom and an impinging O atom or CO molecule from the gas phase, forming O_2 or CO_2, respectively. Hence, the larger f_c, the faster recombination occurs. Note that the O_2 and CO mole fractions stabilize at a lower value for a higher value of f_c. While the rate for recombination between CO and O* is higher than that for O + O*, the ratio between both does not change when f_c is altered. Nevertheless, the effect of the fastest reaction (CO+O*) on the mole fractions becomes more pronounced as both rates are increased by the same factor. Also note that large variations in f_c have only a moderate effect on the CO density in the plasma (i.e., at 0 cm) as the CO fraction roughly doubles when f_c drops from 0.02 to 0.002 and the effect is even smaller when f_c drops further from 0.002 to 0.0002.

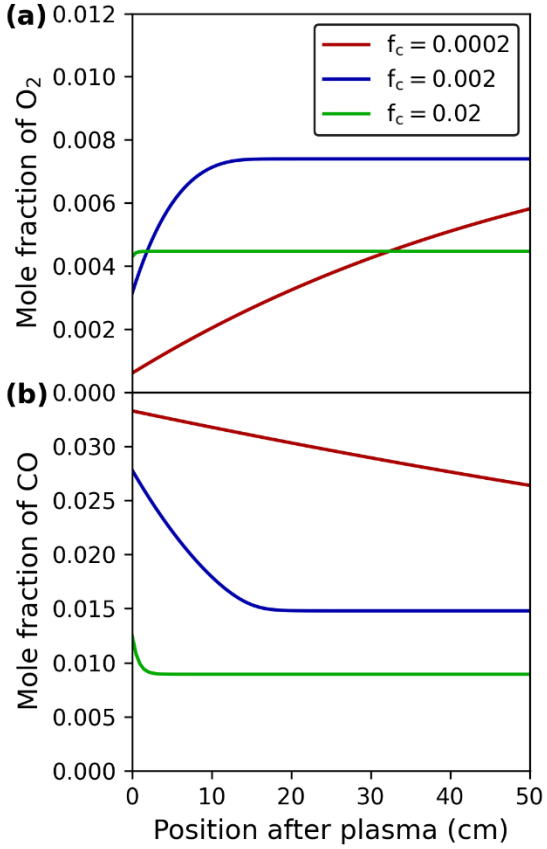

Figure S1. Effect of varying the fraction of chemisorption sites f_c on the mole fractions of O_2 (a) and CO (b). The default value in the model is f_c = 0.002. Conditions: T = 500 K, p = 5 mbar and flow rate = 100 sccm.

The effect of varying the pre-exponential factor for desorption v_d is illustrated in Figure S2. When the default value of v_d is lowered by a factor 10, i.e., from 10^{15} to 10^{14} s^{-1}, the O_2 and CO mole fractions stabilize at slightly higher values. Lowering the pre-exponential factor results in lower rates for desorption from both physisorption and chemisorption sites, but the latter are already largely occupied when $v_d = 10^{15}$ s^{-1}. Hence, lowering v_d from 10^{15} to 10^{14} s^{-1} mainly enhances the coverage of physisorbed O* atoms, which improves the formation of O_2 via the L-H reaction between physisorbed and chemisorbed O* atoms. Since more O atoms recombine to O_2, the mole fraction of CO also stabilizes at a higher value, as less O atoms will be available to recombine with CO to CO_2. When v_d is set to 10^{16} s^{-1}, recombination of O atoms on the surface becomes very slow, as is apparent from the slow evolution of the O_2 and CO mole fractions in the afterglow. This is because desorption from chemisorption sites becomes significant for this value of v_d, thus lowering the coverage of chemisorbed O* atoms, which indicates that a value of 10^{16} s^{-1} for v_d is not realistic.

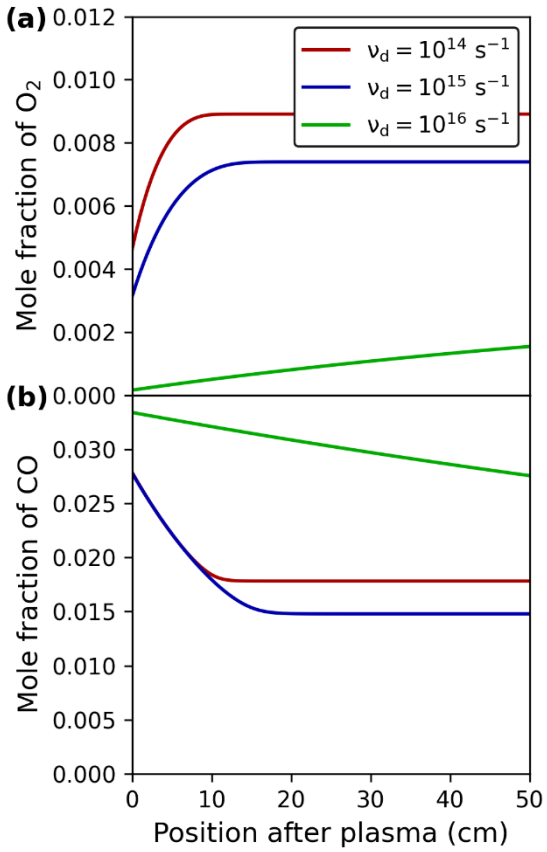

Figure S2. Effect of varying the pre-exponential factor for desorption ν_d on the mole fractions of O_2 (a) and CO (b). The default value in the model is $\nu_d = 10^{15}$ s^{-1}. Conditions: T = 500 K, p = 5 mbar and flow rate = 100 sccm.

Figure S3 illustrates the effect of varying the activation barrier for recombination between two O atoms $E_{r,O+O}$ by a factor 3/2. Naturally, a lower activation barrier improves the reaction rate for O+O recombination, and thus also the O_2 (and CO) mole fractions. When $E_{r,O+O}$ is increased by a factor 3/2, i.e., from 0.13 to 0.20 eV, the O_2 and CO mole fractions at the end of the afterglow are approximately halved. Conversely, when $E_{r,O+O}$ is lowered from 0.13 to 0.087 eV, the O_2 and CO mole fractions at the end of the afterglow rise by approximately 40%. Note that while the O atom fraction in the plasma (at 0 cm) clearly depends on the value of $E_{r,O+O}$, the CO mole fraction in the plasma does not change significantly when $E_{r,O+O}$ is altered.

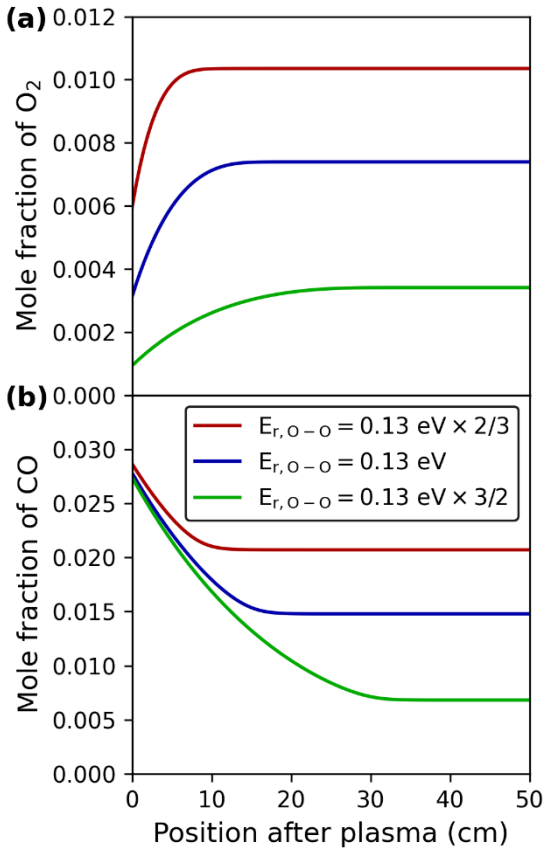

Figure S3. Effect of varying the activation barrier for recombination between O atoms $E_{r,O+O}$ on the mole fractions of O_2 (a) and CO (b). The default value in the model is $E_{r,O+O}$ = 0.13 eV. Conditions: T = 500 K, p = 5 mbar and flow rate = 100 sccm.

Lastly, Figure S4 illustrates the effect of varying the activation barrier for recombination between CO and an adsorbed O* atom. Increasing this activation barrier lowers the rate of the backreaction to CO_2 and thus enhances the O_2 and CO mole fractions. When the value of $E_{r,CO+O}$ is increased by a factor 3/2, i.e., from 0.104 to 0.156 eV, the O_2 and CO mole fractions near the end of the afterglow are enhanced by approximately 55%. Lowering the activation barrier from 0.104 to 0.069 eV reduces the O_2 and CO mole fractions at the end of the afterglow by approximately 35%. Hence, the height of the activation barriers for the recombination reactions has a significant impact on the mole fractions of O_2 and CO, and thus on the CO_2 conversion. Whether most of the O* adsorbed atoms will recombine with impinging O atoms to form O_2, or with CO to form CO_2, eventually depends on the height of the activation barriers of both reactions relative to each other.

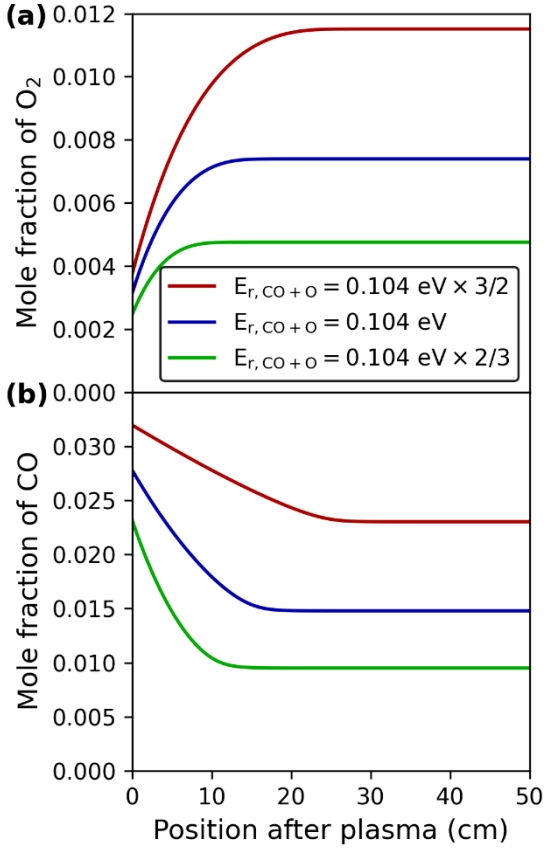

Figure S4. Effect of varying the activation barrier for recombination between CO and an adsorbed O atom $E_{r,cO+O}$ on the mole fractions of O_2 (a) and CO (b). The default value in the model is $E_{r,cO+O}$ = 0.104 eV. Conditions: T = 500 K, p = 5 mbar and flow rate = 100 sccm.*

S5. DFT energies and vibrational frequencies

Table S4. DFT energies and vibrational frequencies of the species involved in reactions on the transition metal surfaces. The energies are calculated as the formation energy of the species relative to CO and O_2 in the gas phase, and the empty slab.

Species	Surface	Energy (eV)	Frequencies (cm^{-1})[a]
CO_2	-	-3.02	[667.0, 667.0, 1333.0, 2349.0][b, 36]
CO	-	0.0	[2143.2] [b, 36]
O_2	-	0.0	[1556.4] [b, 36]
O	-	2.88	[]
*	All	0.0	[]
CO_2*	Ag(111)	-3.21	[50.0, 50.0, 50.0, 50.0, 51.0, 595.8, 610.3, 1298.5, 2305.2]
	Cu(111)	-3.21	[50.0, 50.0, 50.0, 50.0, 50.9, 596.9, 611.0, 1298.3, 2303.5]
	Pd(111)	-3.24	[50.0, 50.0, 50.0, 50.0, 55.1, 592.9, 611.0, 1297.2, 2299.4]
	Rh(111)	-3.24	[50.0, 50.0, 50.0, 50.0, 55.1, 589.0, 608.7, 1296.7, 2298.7]
CO*	Ag(111)	-0.17	[50.0, 50.0, 116.9, 116.9, 137.1, 2035.0]
	Cu(111)	-0.61	[50.0, 50.0, 257.3, 257.4, 296.0, 2002.1]
	Pd(111)	-1.76	[146.5, 147.2, 298.4, 322.6, 323.2, 1749.9]
	Rh(111)	-1.74	[50.0, 50.0, 386.0, 386.0, 430.3, 1966.0]
O_2*	Ag(111)	-0.36	[50.0, 81.8, 85.2, 145.5, 271.6, 1056.2]
	Cu(111)	-1.05	[108.7, 165.4, 192.2, 328.5, 365.7, 626.6]
	Pd(111)	-1.06	[125.3, 191.9, 281.5, 320.2, 414.3, 805.8]
	Rh(111)	-1.69	[138.5, 207.7, 269.3, 361.6, 442.4, 648.8]
O*	Ag(111)	-0.64	[311.1, 311.1, 322.1]
	Cu(111)	-1.78	[370.5, 370.5, 407.2]
	Pd(111)	-1.47	[361.5, 361.5, 398.2]
	Rh(111)	-2.19	[340.8, 340.9, 443.9]
O-O*	Ag(111)	0.40	[69.6, 148.6, 200.4, 259.1, 292. 3]
	Cu(111)	-1.03	[71.1, 268.1, 293.3, 375.8, 406.2]
	Pd(111)	-0.48	[63.3, 152.1, 348.5, 422.8, 537.9]
	Rh(111)	-1.60	[124.2, 221.1, 253.6, 438.9, 526.2]
O-CO*	Ag(111)	-0.75	[50.0, 96.9, 161.7, 225.1, 264.3, 304.3, 418.8, 1955.4]

Cu(111)	-1.80	[50.0, 77.6, 211.2, 297.2, 325.5, 364.0, 519.3, 1930.3]
Pd(111)	-1.78	[50.0, 113.1, 246.6, 309.2, 358.3, 361.5, 500.0, 1951.9]
Rh(111)	-2.59	[56.8, 124.9, 272.6, 278.4, 379.0, 436.3, 568.7, 1874.0]

a) A cut-off of 50.0 cm^{-1} was used as lower boundary for the vibrational frequencies.

b) For gas molecules experimental frequencies taken from the NIST Computational Chemistry Comparison and Benchmark Database[36] were used.

S6. Parameters used in the ideal gas approximation

Table S5. Parameters used in the ideal gas approximation for calculating the enthalpy correction and entropy of gas molecules.

Species	**Geometry**	**I_{rot} (amu Å^2)[36]**	**Mass (amu)[37]**	**Symmetry number**	**Spin multiplicity**
O_2	Linear	11.72561	31.9988	2	1
O	Monoatomic	0.0	15.9994	1	1
CO_2	Linear	43.20143	44.0095	2	0
CO	Linear	8.768466	28.0101	1	0

S7. Parameters used in the modified Arrhenius expression of the surface rate coefficients as a function of temperature

Table S6. List of the parameters acquired by fitting the calculated values of the rate coefficients for surface reactions to a modified Arrhenius expression.

Surface	Reaction	a[a]	b	c
Ag(111)	$O + * \rightarrow O*$	9.094×10^{-14}	5.000×10^{-1}	9.388×10^{-7}
Ag(111)	$O* \rightarrow O + *$	1.387×10^{16}	-5.959×10^{-1}	-4.052×10^{4}
Ag(111)	$O_2 + * \rightarrow O_2*$	6.431×10^{-14}	5.000×10^{-1}	2.871×10^{-6}
Ag(111)	$O_2* \rightarrow O_2 + *$	1.167×10^{20}	-2.011	-4.442×10^{3}
Ag(111)	$CO_2 + * \rightarrow CO_2*$	5.483×10^{-14}	5.000×10^{-1}	-6.286×10^{-6}
Ag(111)	$CO_2* \rightarrow CO_2 + *$	8.318×10^{18}	-2.086	-2.350×10^{3}
Ag(111)	$CO + * \rightarrow CO*$	6.873×10^{-14}	5.000×10^{-1}	5.979×10^{-6}
Ag(111)	$CO* \rightarrow CO + *$	1.180×10^{19}	-1.933	-1.991×10^{3}
Ag(111)	$O_2* + * \rightarrow O* + O*$	4.372×10^{12}	4.897×10^{-1}	-1.910×10^{4}
Ag(111)	$O* + O* \rightarrow O_2* + *$	6.869×10^{10}	4.670×10^{-1}	-8.263×10^{3}
Ag(111)	$CO_2* + * \rightarrow CO* + O*$	1.350×10^{12}	-7.697×10^{-2}	-7.121×10^{2}
Ag(111)	$CO* + O* \rightarrow CO_2* + *$	5.859×10^{8}	9.106×10^{-1}	-2.723×10^{4}
Cu(111)	$O + * \rightarrow O*$	9.094×10^{-14}	5.000×10^{-1}	1.587×10^{-5}
Cu(111)	$O* \rightarrow O + *$	6.182×10^{15}	-4.112×10^{-1}	-5.361×10^{4}
Cu(111)	$O_2 + * \rightarrow O_2*$	6.431×10^{-14}	5.000×10^{-1}	-2.305×10^{-5}
Cu(111)	$O_2* \rightarrow O_2 + *$	1.705×10^{21}	-1.969	-1.257×10^{4}
Cu(111)	$CO_2 + * \rightarrow CO_2*$	5.483×10^{-14}	5.000×10^{-1}	4.972×10^{-7}
Cu(111)	$CO_2* \rightarrow CO_2 + *$	8.325×10^{18}	-2.086	-2.350×10^{3}
Cu(111)	$CO + * \rightarrow CO*$	6.873×10^{-14}	5.000×10^{-1}	1.360×10^{-5}
Cu(111)	$CO* \rightarrow CO + *$	1.762×10^{19}	-1.676	-6.924×10^{3}
Cu(111)	$O_2* + * \rightarrow O* + O*$	6.720×10^{12}	3.619×10^{-1}	-2.902×10^{4}
Cu(111)	$O* + O* \rightarrow O_2* + *$	6.683×10^{12}	3.377×10^{-2}	-1.349×10^{2}
Cu(111)	$CO_2* + * \rightarrow CO* + O*$	2.921×10^{12}	8.546×10^{-2}	-6.746×10^{3}
Cu(111)	$CO* + O* \rightarrow CO_2* + *$	1.237×10^{9}	6.955×10^{-1}	-1.523×10^{4}
Pd(111)	$O + * \rightarrow O*$	9.094×10^{-14}	5.000×10^{-1}	1.587×10^{-5}
Pd(111)	$O* \rightarrow O + *$	6.780×10^{15}	-4.325×10^{-1}	-5.003×10^{4}
Pd(111)	$O_2 + * \rightarrow O_2*$	6.431×10^{-14}	5.000×10^{-1}	-2.305×10^{-5}
Pd(111)	$O_2* \rightarrow O_2 + *$	7.679×10^{20}	-1.734	-1.245×10^{4}
Pd(111)	$CO_2 + * \rightarrow CO_2*$	5.483×10^{-14}	5.000×10^{-1}	4.972×10^{-7}

Pd(111)	$CO_2^* \rightarrow CO_2 + *$	9.148×10^{18}	-2.089	-2.705×10^{3}
Pd(111)	$CO + * \rightarrow CO^*$	6.873×10^{-14}	5.000×10^{-1}	1.360×10^{-5}
Pd(111)	$CO^* \rightarrow CO + *$	9.200×10^{19}	-1.555	-2.033×10^{4}
Pd(111)	$O_2^* + * \rightarrow O^* + O^*$	6.369×10^{12}	3.718×10^{-1}	-2.827×10^{4}
Pd(111)	$O^* + O^* \rightarrow O_2^* + *$	2.371×10^{12}	3.206×10^{-1}	-6.419×10^{3}
Pd(111)	$CO_2^* + * \rightarrow CO^* + O^*$	1.354×10^{13}	1.305×10^{-1}	-1.686×10^{4}
Pd(111)	$CO^* + O^* \rightarrow CO_2^* + *$	1.100×10^{9}	6.379×10^{-1}	-1.587×10^{4}
Rh(111)	$O + * \rightarrow O^*$	9.094×10^{-14}	5.000×10^{-1}	1.587×10^{-5}
Rh(111)	$O^* \rightarrow O + *$	6.488×10^{15}	-4.281×10^{-1}	-5.838×10^{4}
Rh(111)	$O_2 + * \rightarrow O_2^*$	6.431×10^{-14}	5.000×10^{-1}	-2.305×10^{-5}
Rh(111)	$O_2^* \rightarrow O_2 + *$	1.236×10^{21}	-1.780	-1.983×10^{4}
Rh(111)	$CO_2 + * \rightarrow CO_2^*$	5.483×10^{-14}	5.000×10^{-1}	4.972×10^{-7}
Rh(111)	$CO_2^* \rightarrow CO_2 + *$	9.403×10^{18}	-2.094	-2.710×10^{3}
Rh(111)	$CO + * \rightarrow CO^*$	6.873×10^{-14}	5.000×10^{-1}	1.360×10^{-5}
Rh(111)	$CO^* \rightarrow CO + *$	6.015×10^{18}	-1.381	-1.981×10^{4}
Rh(111)	$O_2^* + * \rightarrow O^* + O^*$	2.587×10^{12}	3.890×10^{-1}	-3.196×10^{4}
Rh(111)	$O^* + O^* \rightarrow O_2^* + *$	1.693×10^{12}	2.839×10^{-1}	-7.974×10^{2}
Rh(111)	$CO_2^* + * \rightarrow CO^* + O^*$	1.189×10^{12}	1.892×10^{-1}	-1.535×10^{4}
Rh(111)	$CO^* + O^* \rightarrow CO_2^* + *$	1.587×10^{9}	5.136×10^{-1}	-6.536×10^{3}

a) Units are $cm^3\ s^{-1}$ for adsorption reactions and s^{-1} for other surface reactions.

S8. Effect of the free translator vs. harmonic oscillator approximation on the kinetics of plasma-catalytic CO_2 splitting

As discussed in section 2.2.5. of the main paper, we use the harmonic oscillator approximation[38] to calculate the entropy of the surface species, as well as their change in enthalpy with temperature. The harmonic oscillator approximation treats all degrees of freedom of the surface species as vibrational modes, corresponding to an adsorbate that oscillates within a surface site. Naturally, this results in a relatively low estimate of the adsorbate entropies. Another limiting case is the free translator approximation in which the surface species are assumed to retain two translational degrees of freedom, i.e. corresponding to an adsorbate that moves freely on the surface. Consequently, this approximation results in a larger estimate of the adsorbate entropies, and thus more stable surface species (i.e., lower Gibbs free energies) especially at high temperature.

To illustrate the effect of using the free translator approximation, we here discuss the results for plasma-catalytic CO_2 splitting with an Ag catalyst at 1100 K, 5 mbar and a flow rate of 100 sccm, i.e., the same conditions as used in Figure 6 of the main paper. To calculate the enthalpy correction and entropy using the free translation approximation, the two vibrational modes with the lowest vibrational frequencies of each surface species were replaced by translational modes. The contribution of the two translational modes to the enthalpy correction and entropy were calculated as two-third of the total translational contribution used in the ideal gas approximation[38] (i.e., which accounts for three translational degrees of freedom). Note that the contribution of the remaining vibrational modes to the enthalpy correction and entropy were still included in the total enthalpy correction and entropy.

Figure S5 shows the calculated mole fractions of gas species (a), fractional surface coverages (b), O atom loss rates (c) and net surface rates (d) for a CO_2 plasma afterglow in contact with a catalytic Ag surface, when the free translator approximation is used. For comparison, Figure 6 in the main paper shows the results of the corresponding simulation when the harmonic oscillator approximation is used. As can be seen in Figure S5 (a), the decline of the CO and O_2 mole fractions following the depletion of the O atoms in the gas phase is much faster when the free translator approximation is used, compared to the harmonic oscillator approximation (Figure 6 (a) in the main paper). Indeed, the free translator approximation results in higher adsorbate entropies, and thus more stable surface species (i.e., lower Gibbs free energies of formation), especially at high temperature. This makes desorption of the adsorbed molecules more difficult and enhances the dissociation of adsorbates on the surface, as dissociation results in a net gain of two translational degrees of freedom. Consequently, the thermal catalytic oxidation of CO is enhanced, as its rate-determining step on Ag, namely O_2* dissociation, becomes easier.

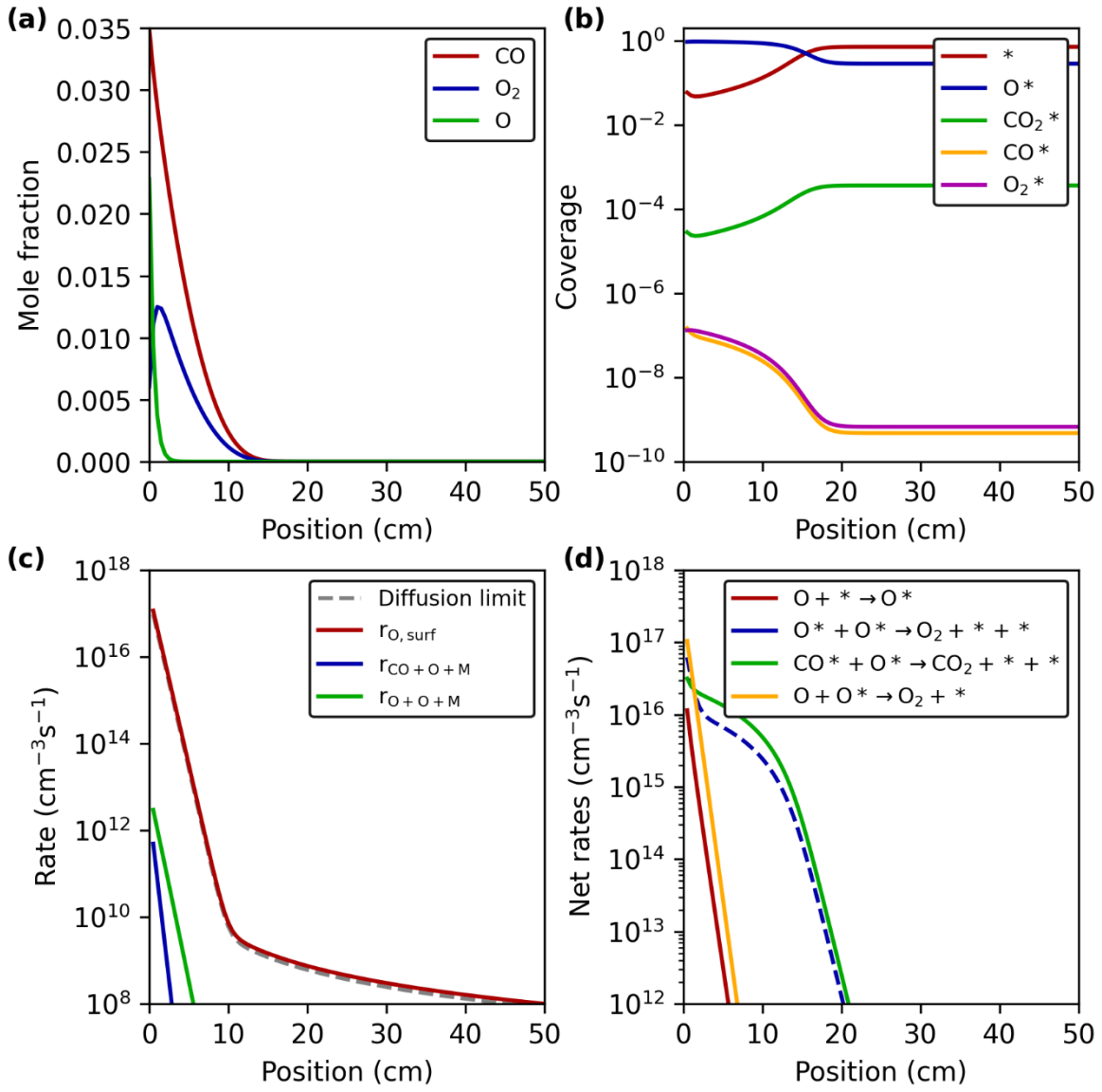

Figure S5. Mole fractions (a), fractional surface coverages (b), O atom loss rates (c), and net surface rates (d) of a CO_2 plasma afterglow in contact with an Ag surface, when using the free translator approximation to calculate the enthalpy corrections and entropies of the surface species. The dashed line in (d) indicates a negative net rate, corresponding to the reverse reaction, i.e., dissociation of O_2. Conditions: T = 1100 K, p = 5 mbar and flow rate = 100 sccm.*

The effect of the more difficult desorption and easier dissociation on the surface can also be observed in the surface coverages in Figure S5 (b). Indeed, the surface coverages increase upon switching from the harmonic oscillator to the free translator approximation (Figures 6 (b) in the main paper and Figure S5 (b), respectively). Especially the coverage of O* rises strongly and O* even covers most of the surface before depletion of the O atoms in the gas phase.

While the use of the free translator approximation significantly affects the surface kinetics, the flux and net consumption of O atoms on the surface remain largely the same compared to the harmonic oscillator

approximation (Figure S5 (c) and Figure 6 (c), respectively). In both cases most O atom recombination occurs almost exclusively via surface reactions and the loss of O atoms at the surface is limited by diffusion to the surface.

Figure S5 (d) illustrates the net reaction rates for loss of O atoms on the Ag surface. Note that in line with Figure 6 (d) (main paper), the dashed (blue) line of O*+O* recombination indicates a negative net rate, and thus corresponds to the reverse reaction, i.e., dissociation of O_2*. Interestingly, due to the more facile dissociation of O_2* with the free translator approximation, it becomes easier for O_2, which is formed at the surface, to re-adsorb and dissociate into O* than for O atoms to diffuse to the surface and adsorb. Instead, the O atoms that reach the surface will now react with O* via an L-R reaction to form O_2, of which a fraction adsorbs and dissociates again to form adsorbed O*. This arises from the diffusion limitation between the bulk gas and the surface, which limits the loss rate of O atoms to the surface. Because O_2 is formed at the surface, its adsorption rate is not limited by diffusion to the surface. Hence, despite resulting in higher O* coverages, the free translator approximation reduces the net rate of O* recombination via the L-H reaction, as this results in a larger entropy loss (i.e., corresponding to two translational degrees of freedom) upon going from two adsorbates (O*+O*) to one (O_2*). The rate of the L-R reaction, however, is increased due to the higher O* coverages and L-R becomes the main process for O atom recombination (Figure S5 (d)). However, the rate coefficient used for the L-R reaction (Eq. (10) in the main paper) only includes an enthalpy barrier in the sticking coefficient, while the pre-exponential factor (i.e., the Hertz-Knudsen equation) only accounts for the loss of one translational degree of freedom of the impinging atom. Hence, any loss of entropy of the adsorbate between the initial and transition state is not considered.

Finally, the rates of O_2* dissociation and recombination between O* and CO* to form CO_2* are initially higher when the free translation approximation is used (Figure S5 (d)), compared to when the harmonic oscillator approximation is used (Figure 6 (d) in the main paper), as is also evident from the evolution of the O_2 and CO mole fractions in panel (a) of both figures. However, due to the faster decline of the mole fractions of these gas species in Figure S5 (a), the rates of O_2* dissociation and CO*+O* recombination in Figure S5 (d) also drop rapidly, around 15 cm after the plasma.

To conclude, the use of the free translator approximation results in easier O_2* dissociation, and thus faster thermal-catalytic CO* oxidation to CO_2*, which gives rise to a quick drop of the CO* and O_2* mole fractions after depletion of O atoms in the gas phase.

S9. References

(1) Burcat, a; Branko, R. *Third Millennium Ideal Gas and Condensed Phase Thermochemical Database for Combustion with Updates from Active Thermochemical Tables*; 2005.

(2) McBride, B. J.; Zehe, M. J.; Gordon, S. *NASA Glenn Coefficients for Calculating Thermodynamic Properties of Individual Species*; 2002.

(3) Obtained from LXCAT (IST-Lisbon database) www.lxcat.net.

(4) Obtained from LXCAT (Morgan database) www.lxcat.net.

(5) Obtained from LXCAT (Itikawa database) www.lxcat.net.

(6) Polak, L. S.; Slovetsky, D. I. Electron Impact Induced Electronic Excitation and Molecular Dissociation. *Int. J. Radiat. Phys. Chem.* **1976**, *8* (1–2), 257–282. https://doi.org/10.1016/0020-7055(76)90070-X.

(7) Obtained from LXCAT (Biagi database) www.lxcat.net.

(8) Capitelli, M.; Ferreira, C. M.; Gordiets, B. F.; Osipov, A. I. *Plasma Kinetics in Atmospheric Gases*; Springer Series on Atomic, Optical, and Plasma Physics; Springer Berlin Heidelberg: Berlin, Heidelberg, 2000; Vol. 31. https://doi.org/10.1007/978-3-662-04158-1.

(9) Kossyi, I. A.; Kostinsky, A. Y.; Matveyev, A. A.; Silakov, V. P. Kinetic Scheme of the Non-Equilibrium Discharge in Nitrogen-Oxygen Mixtures. *Plasma Sources Sci. Technol.* **1992**, *1* (3), 207–220. https://doi.org/10.1088/0963-0252/1/3/011.

(10) Tsang, W.; Hampson, R. F. Chemical Kinetic Data Base for Combustion Chemistry. Part I. Methane and Related Compounds. *J. Phys. Chem. Ref. Data* **1986**, *15* (3), 1087–1279. https://doi.org/10.1063/1.555759.

(11) Park, C. A Review of Reaction Rates in High Temperature Air. In *24th Thermophysics Conference*; American Institute of Aeronautics and Astronautics: Reston, Virigina, 1989. https://doi.org/10.2514/6.1989-1740.

(12) Belostotsky, S. G.; Economou, D. J.; Lopaev, D. V.; Rakhimova, T. V. Negative Ion Destruction by $O(^3P)$ Atoms and $O_2(a\ ^1\Delta_g)$ Molecules in an Oxygen Plasma. *Plasma Sources Sci. Technol.* **2005**, *14* (3), 532–542. https://doi.org/10.1088/0963-0252/14/3/016.

(13) Atkinson, R.; Baulch, D. L.; Cox, R. A.; Crowley, J. N.; Hampson, R. F.; Hynes, R. G.; Jenkin, M. E.; Rossi, M. J.; Troe, J. Evaluated Kinetic and Photochemical Data for Atmospheric Chemistry: Volume I - Gas Phase Reactions of Ox, HOx, NOx and SOx Species. *Atmos. Chem. Phys.* **2004**, *4* (6), 1461–1738. https://doi.org/10.5194/acp-4-1461-2004.

(14) Lifshitz, C.; Wu, R. L. C.; Haartz, J. C.; Tiernan, T. O. Associative Detachment Reactions of Negative Ions with O_3. *J. Chem. Phys.* **1977**, *67* (5), 2381–2382. https://doi.org/10.1063/1.435078.

(15) Stafford, D. S.; Kushner, M. J. $O_2(^1\Delta)$ Production in He/O_2 Mixtures in Flowing Low Pressure Plasmas. *J. Appl. Phys.* **2004**, *96* (5), 2451–2465. https://doi.org/10.1063/1.1768615.

(16) Gudmundsson, J. T.; Thorsteinsson, E. G. Oxygen Discharges Diluted with Argon: Dissociation Processes. *Plasma Sources Sci. Technol.* **2007**, *16* (2), 399–412. https://doi.org/10.1088/0963-0252/16/2/025.

(17) Thomas G. Beuthe, T. G. B.; Jen-Shih Chang, J.-S. C. Chemical Kinetic Modelling of Non-Equilibrium Ar-CO_2 Thermal Plasmas. *Jpn. J. Appl. Phys.* **1997**, *36* (7S), 4997–5002. https://doi.org/10.1143/JJAP.36.4997.

(18) Park, C.; Howe, J. T.; Jaffe, R. L.; Candler, G. V. Review of Chemical-Kinetic Problems of Future NASA Missions, II: Mars Entries. *J. Thermophys. Heat Transf.* **1994**, *8* (1), 9–23. https://doi.org/10.2514/3.496.

(19) Dean, A. J.; Davidson, D. F.; Hanson, R. K. A Shock Tube Study of Reactions of C Atoms with H_2 and O_2 Using Excimer Photolysis of C_3O_2 and C Atom Atomic Resonance Absorption Spectroscopy. *J. Phys. Chem.* **1991**, *95* (1), 183–191. https://doi.org/10.1021/j100154a037.

(20) Petuchowski, S. J.; Dwek, E.; Allen, J. E., J.; Nuth, J. A., I. CO Formation in the Metal-Rich Ejecta of SN 1987A. *Astrophys. J.* **1989**, *342*, 406. https://doi.org/10.1086/167601.

(21) Prasad, S. S.; Huntress, W. T., J. A Model for Gas Phase Chemistry in Interstellar Clouds. I - The Basic Model, Library of Chemical Reactions, and Chemistry among C, N, and O Compounds. *Astrophys. J. Suppl. Ser.* **1980**, *43*, 1–35. https://doi.org/10.1086/190665.

(22) Albritton, D. L. Ion-Neutral Reaction-Rate Constants Measured in Flow Reactors through 1977. *At. Data Nucl. Data Tables* **1978**, *22* (1), 1–89. https://doi.org/10.1016/0092-640X(78)90027-X.

(23) Arin, L. M.; Warneck, P. Reaction of Ozone with Carbon Monoxide. *J. Phys. Chem.* **1972**, *76* (11), 1514–1516. https://doi.org/10.1021/j100655a002.

(24) McFarland, M.; Albritton, D. L.; Fehsenfeld, F. C.; Ferguson, E. E.; Schmeltekopf, A. L. Flow-Drift Technique for Ion Mobility and Ion-Molecule Reaction Rate Constant Measurements. III. Negative Ion Reactions of O^- with CO, NO, H_2, and D_2. *J. Chem. Phys.* **1973**, *59* (12), 6629–6635. https://doi.org/10.1063/1.1680043.

(25) Fehsenfeld, F. C.; Ferguson, E. E. Thermal Energy Reaction Rate Constants for H+ and CO+ with O and NO. *J. Chem. Phys.* **1972**, *56* (6), 3066–3070. https://doi.org/10.1063/1.1677642.

(26) Adams, N. G.; Smith, D.; Grief, D. Reactions of H_nCO^+ Ions with Molecules at 300 K. *Int. J. Mass Spectrom. Ion Phys.* **1978**, *26* (4), 405–415. https://doi.org/10.1016/0020-7381(78)80059-X.

(27) Husain, D.; Young, A. N. Kinetic Investigation of Ground State Carbon Atoms, C(2^3P_J). *J. Chem. Soc. Faraday Trans. 2* **1975**, *71* (February), 525. https://doi.org/10.1039/f29757100525.

(28) Fahey, D. W.; Fehsenfeld, F. C.; Ferguson, E. E. Rate Constant for the Reaction $C^+ + CO_2$ at Collision Energies 0.04 to 2.5eV. *Geophys. Res. Lett.* **1981**, *8* (10), 1115–1117. https://doi.org/10.1029/GL008i010p01115.

(29) Burmeister, M.; Roth, P. ARAS Measurements on the Thermal Decomposition of CO_2 behind Shock Waves. *AIAA J.* **1990**, *28* (3), 402–405. https://doi.org/10.2514/3.10406.

(30) Cenian, A.; Chernukho, A.; Borodin, V.; Śliwiński, G. Modeling of Plasma-Chemical Reactions in Gas Mixture of CO_2 Lasers I. Gas Decomposition in Pure CO_2 Glow Discharge. *Contrib. to Plasma Phys.* **1994**, *34* (1), 25–37. https://doi.org/10.1002/ctpp.2150340105.

(31) Abreu, V. J.; Yee, J. H.; Solomon, S. C.; Dalgarno, A. The Quenching Rate of O(^{1}D) by O(^{3}P). *Planet. Space Sci.* **1986**, *34* (11), 1143–1145. https://doi.org/10.1016/0032-0633(86)90026-7.

(32) Tully, J. C. Reactions of O(^{1}D) with Atmospheric Molecules. *J. Chem. Phys.* **1975**, *62* (5), 1893–1898. https://doi.org/10.1063/1.430675.

(33) Dunlea, E. J.; Ravishankara, A. R. Kinetic Studies of the Reactions of O(^{1}D) with Several Atmospheric Molecules. *Phys. Chem. Chem. Phys.* **2004**, *6* (9), 2152–2161. https://doi.org/10.1039/b400247d.

(34) Beverly, R. E. Ion Aging Effects on the Dissociative-Attachment Instability in CO_2 Lasers. *Opt. Quantum Electron.* **1982**, *14* (6), 501–513. https://doi.org/10.1007/BF00610306.

(35) Shields, H.; Smith, A. L. S.; Norris, B. Negative Ion Effects in TEA CO_2 Lasers. *J. Phys. D: Appl. Phys.* **1976**, *9* (11), 1587–1603. https://doi.org/10.1088/0022-3727/9/11/007.

(36) Russell D. Johnson III. NIST Computational Chemistry Comparison and Benchmark Database, NIST Standard Reference Database Number 101 http://cccbdb.nist.gov/ (accessed Dec 22, 2024).

(37) *NIST Chemistry WebBook, NIST Standard Reference Database Number 69*; Linstrom, P. J., Mallard, W. G., Eds.; National Institute of Standards and Technology: Gaithersburg MD, 20899. https://doi.org/10.18434/T4D303.

(38) Larsen, A. H.; Mortensen, J. J.; Blomqvist, J.; Castelli, I. E.; Christensen, R.; Dułak, M.; Friis, J.; Groves, M. N.; Hammer, B.; Hargus, C.; Hermes, E. D.; Jennings, P. C.; Jensen, P. B.;

Kermode, J.; Kitchin, J. R.; Kolsbjerg, E. L.; Kubal, J.; Kaasbjerg, K.; Lysgaard, S.; Bergmann Maronsson, J.; Maxson, T.; Olsen, T.; Pastewka, L.; Peterson, A.; Rostgaard, C.; Schiøtz, J.; Schütt, O.; Strange, M.; Thygesen, K. S.; Vegge, T.; Vilhelmsen, L.; Walter, M.; Zeng, Z.; Jacobsen, K. W. The Atomic Simulation Environment—a Python Library for Working with Atoms. *J. Phys. Condens. Matter* **2017**, *29* (27), 273002. https://doi.org/10.1088/1361-648X/aa680e.